Acentric chromosome congression and alignment on the metaphase plate occur via kinetochore-independent forces

Abstract

Chromosome congression and alignment on the metaphase plate involves lateral and microtubule plus-end interactions with the kinetochore. Here we take advantage of our ability to efficiently generate a GFP-marked acentric X chromosome fragment in *Drosophila* neuroblasts to identify forces acting on chromosome arms that drive congression and alignment. We find acentrics efficiently align on the metaphase plate, often more rapidly than kinetochore-bearing chromosomes. Unlike intact chromosomes, the paired sister acentrics oscillate as they move to and reside on the metaphase plate in a plane distinct and significantly further from the main mass of intact chromosomes. Consequently, at anaphase onset acentrics are oriented either parallel or perpendicular to the spindle. Parallel-oriented sisters separate by sliding while those oriented perpendicularly separate via unzipping. This oscillation, together with the fact that in monopolar spindles acentrics are rapidly shunted away from the poles, indicates that distributed plus-end directed forces are primarily responsible for acentric migration. This conclusion is supported by the observation that reduction of EB1 preferentially disrupts acentric alignment. In addition, reduction of Klp3a activity, a gene required for the establishment of pole-to-pole microtubules, preferentially disrupts acentric alignment. Taken together these studies suggest that plus-end forces mediated by the outer pole-to-pole microtubules are primarily responsible for acentric metaphase alignment. Surprisingly, we find that a small fraction of sister acentrics are anti-parallel aligned indicating that the kinetochore is required to ensure parallel alignment of sister chromatids. Finally, we find induction of acentric chromosome fragments results in a global reorganization of the congressed chromosomes into a torus configuration.

Introduction

Chromosome fragments lacking a centromere and a telomere are known as acentrics. Due to their lack of a kinetochore, acentrics are unable to make canonical attachments to microtubules. Kinetochore-microtubule interactions play key roles in mediating chromosome congression to the spindle equator, alignment on the metaphase plate, sister chromosome separation during the metaphase-to-anaphase transition and segregation during anaphase [Navarro & Cheeseman, 2021]. Thus, acentrics might be expected to fail to align properly on the metaphase plate, display separation and segregation defects in anaphase resulting in exclusion from daughter nuclei and the formation of micronuclei [Kanda & Wahl, 2000; LaFountain et al., 2001; Fenech et al., 2011]. However, these expectations are contradicted by the finding that acentric chromosome fragments often display proper sister chromosome separation, poleward migration, and inclusion into daughter nuclei [Royou et al., 2010; Bajer, 1958; Kanda et al., 1998; Vicars et al., 2021; Karg et al., 2017; Bretscher & Fox, 2016; Karg et al., 2015; Warecki & Sullivan, 2018; Khodjakov et al., 1996; Liang et al., 1993; Warecki et al., 2020]. Proposed mechanisms include neo-centromere formation and direct association of acentrics with microtubules or a kinetochore-bearing chromosome [Ishii et al., 2008; Platero et al., 1999, Kanda et al., 2001; Ohno et al., 2016; Karg et al., 2017; Warecki & Sullivan, 2020]. Studies have shown that separation of sister acentric chromosomes during early anaphase relies on Topoisomerase II activity as well as microtubule plus-end pushing forces [Vicars et al., 2021]. Additional work has shown that the anaphase poleward segregation of acentric chromosomes involves Klp3a mediated microtubule-based movement [Karg et al., 2017].

Here we explore the mechanisms that drive congression and alignment of acentric chromosome fragments at the metaphase plate as this also provides insight into the non-kinetochore forces driving congression of intact chromosomes. As with sister chromosome separation and segregation, the kinetochore plays a key role in chromosome congression and alignment on the metaphase plate [Barisic et al., 2014; Ye et al., 2015; Chmatal et al., 2015].

Following nuclear-envelope breakdown, chromosomes positioned within the microtubule arc emanating from opposing centrosomes quickly establish lateral interactions with the plus-end kinetochore-associated motor protein CENP-E (kinesin-7) and are transported to the metaphase plate [Yen, 1992; McEwen et al., 2001; Kapoor et al., 2006]. This is referred to as direct congression. Polar ejection forces mediated by plus-end microtubule dynamics and chromokinesins acting on the chromosomes also drive chromosomes away from the poles toward the equator [Maiato et al., 2017; Tanaka, 2008]. Once at the equator, lateral interactions are converted to plus-end microtubule interactions and the sister kinetochores establish biorientation with microtubules attached to opposing poles [Krenn & Musacchio, 2015]. Opposing forces at the sister kinetochores and chromosome arms result in oscillations but maintain the chromosomes at the metaphase plate. Congression of chromosomes located at the spindle periphery and outside of the arc described by the opposing centrosomes and the metaphase plate require an additional step, known as peripheral congression. Chromosomes must first rely on kinetochore-associated Dynein for microtubule minus-end directed transport to the spindle pole. Once at the pole, the chromosomes engage kinetochore kinesin CENP-E for transport to the metaphase plate. [McEwen et al., 2001; Kapoor et al., 2006].

Despite the key role of the kinetochore in driving chromosome movement, acentric chromosome fragments are capable of moving toward and aligning on the metaphase plate [Carlson, 1938a; Royou et al., 2010; Kaye et al., 2004; Bajer, 1958; Vicars et al., 2021; Karg et al., 2017; Rieder et al., 1986]. This was dramatically demonstrated through live analysis of acentric fragments generated via laser ablation. These fragments rapidly moved away from the poles at a rate similar to intact chromosomes [Rieder et al., 1986]. Subsequent live analysis of X-chromosome acentric fragments generated through endonuclease induction in *Drosophila* neuroblasts revealed they also experience robust anti-poleward forces and are capable of aligning on the metaphase plate [Royou et al., 2010; Vicars et al., 2021; Karg et al., 2017; Warecki et al., 2020].

Left unresolved are the mechanisms driving congression and metaphase plate alignment of chromosome fragments lacking a kinetochore. Here we explore this issue by taking advantage of our ability to efficiently generate GFP-labeled acentric fragments in the genetically tractable *Drosophila* neuroblasts. The GFP tag enables us to distinguish the acentric from the kinetochore bearing chromosomes and facilitates tracking of the acentric as it moves to and aligns on the metaphase plate. We find acentrics efficiently align on the metaphase plate more rapidly than kinetochore-bearing chromosomes. Multiple lines of evidence indicate that proper acentric alignment on the metaphase plate relies on pole-to-pole microtubules and plus-end directed microtubule-based forces. Surprisingly, we find that a small but significant fraction of sister acentrics exhibit an anti-parallel alignment. This suggests that the kinetochore is required to ensure parallel alignment of sister chromatids. In addition, we discovered that induction of acentric chromosome fragments results in a global reorganization of the congressed chromosomes into a torus configuration.

Results

Acentric sister chromatids undergo rapid movement at the metaphase plate

As previously described, acentric chromosome fragments have a remarkable ability to congress to the metaphase plate, separate and segregate from one another in anaphase, and incorporate into the reforming daughter nuclei, all while lacking canonical kinetochore-microtubule attachments [Vicars et al., 2021; Warecki et al., 2020]. However, it has been difficult to track an unmarked acentric chromosome fragment during congression and metaphase alignment when the acentric is embedded within the entire chromosome complement. Here we address this issue by taking advantage of a GFP-marker that specifically tags the *Drosophila* X chromosome. In *Drosophila*, the male-specific lethal (MSL3) complex plays a major role in dosage compensation by upregulating genes on the male X chromosome [Sural et al., 2008]. MSL3-GFP preferentially binds the male X euchromatin and thus is suitable for distinguishing

106 the X chromosome from the other chromosomes in live studies. Acentrics are generated using
107 heat-shock-induced expression of the I-CreI endonuclease, which targets rDNA repeats
108 embedded in the X-chromosome centric heterochromatin [Rong et al., 2002; Maggert & Golic,
109 2005; Paredes & Maggert, 2009; Golic & Golic, 2011]. This produces a kinetochore-bearing
110 heterochromatic chromosome fragment and a euchromatic acentric chromosome fragment. As
111 MSL3-GFP specifically localizes to the euchromatin, it preferentially labels the acentric
112 chromosome fragment and is readily tracked over the course of a mitotic division (Figure 1). The
113 MSL3-GFP marker does not disrupt acentric chromosome alignment, segregation, or
114 micronuclei formation when compared to control cells with acentrics alone. In control cells
115 expressing MSL3-GFP but not I-CreI, all of the intact X-chromosomes align normally (N=10).
116 Upon I-CreI induction, 95% (N=18) of the GFP-marked acentrics align on the metaphase plate
117 like intact chromosomes.
118 Live analysis 80 seconds prior to anaphase onset was performed to determine the rate
119 on which intact and acentric chromosomes move to the metaphase plate (Table 1, see
120 accompanying schematic). This analysis reveals that on average acentric X chromosomes
121 move at a significantly faster rate while actively aligning at the metaphase plate (11.7 ± 3.5
122 nm/s, N=14) when compared to intact X chromosomes (8.4 ± 3.3 nm/s, N=12, P=0.01, Mann-
123 Whitney U Test) (Table 1). Intact autosomes (8.5 ± 2.4 nm/s, N=28) align at the metaphase
124 plate at a rate in accordance with the intact X chromosomes (8.4 ± 3.3 nm/s, N=12, P=0.6,
125 Mann-Whitney U Test) (Table 1).
126
127 **Acentric induction causes a global reorganization of congressed chromosomes such**
128 **that acentrics localize to the periphery of the main chromosome mass**
129 Three-dimensional rendering of metaphase images of labeled intact X chromosomes
130 reveal that they are aligned with the autosomes in a planar columnar configuration (Figure 2A,
131 N=5). In addition, the intact X chromosome is consistently positioned at the outer edge of the

column of congressed chromosomes (Figure 2A, N=5). Unexpectedly, we found that I-CreI induction of the acentric X chromosome results in a global reorganization of the congressed chromosomes. Rather than organized in a columnar configuration, the chromosomes are organized into a distinct torus with an absence of chromatin in the center (Figure 2B, N=5). We quantified this global organization by measuring the circularity of the entire congressed mass of chromosomes at metaphase. Using the circularity function in ImageJ, we define perfect circles as having a circularity of 1. The circularity measurements demonstrate that the columnar formations in cells in which I-CreI is not expressed are significantly distinct from the torus shapes seen in neuroblasts expressing I-CreI (Figure 2C). The average circularity of metaphase congressed chromosomes with and without acentrics is 0.95 (SD=0.013, N=6) and 0.44 (SD=0.183, N=6), respectively (Figure 2C).

As with the intact X chromosome, the acentric is peripherally localized. However, the extent to which the acentric X is positioned away from the main chromosome mass is much greater than that of the intact X chromosome. We quantified peripheral positioning by calculating the distance of the intact X chromosome and acentric from the center of chromosome mass (Figure 2C). On average, acentric X chromosomes are positioned significantly farther (3.60 ± 1.34 μm, N=14) from the chromosomal mass center when compared to intact X chromosomes (1.89 ± 0.74 μm, N=16, P=0.01, Mann-Whitney U Test). The center of the mass of chromosomes is determined by defining the upper, lower, left, and right boundaries of the chromosome mass and calculating the center point. Thus, while the acentric X chromosome fragments efficiently congress to the metaphase plate, they reside in a position distinct from the main chromosome complement (Figure 2).

Acentrics oscillate while aligning on the metaphase plate

In prometaphase, kinetochore-bearing replicated sister chromosomes remain paired while congressing to the metaphase plate. This is due to the presence of cohesin protein complexes and DNA catenations between sisters [Guacci et al., 1997; Michaelis et al., 1997; Porter & Farr, 2004]. Similarly, sister acentric X chromosome fragments travel to the metaphase plate as a pair, held together via cohesin and DNA catenations [Vicars et al., 2021].

Previous work demonstrated that the orientation of sister acentrics at the metaphase-to-anaphase transition correlates with their mode of separation during late anaphase [Vicars et al., 2021]. Congressed intact chromosomes always align on the metaphase plate perpendicular to the spindle. In contrast, sister acentrics align either perpendicular or parallel to the spindle. Sister acentrics aligned perpendicular to the spindle, separate via unzipping from one another, while those aligned parallel to the spindle slide past one another to opposing poles. Here we provide insight into the trajectories and mechanisms that result in acentrics reaching the plate in multiple orientations. We discovered that acentrics oscillate while aligning on the metaphase plate. To quantify this, we measure the orientation angles of acentric and intact X chromosomes with respect to the cell equator at 5 second intervals during the 80-second interval prior to anaphase onset (Figure 3).

Kinetochore-bearing sister chromatids align at the metaphase plate undergoing no oscillations, most often remaining perpendicular to the mitotic spindle (Figure 3A, 3C). However, acentric sisters oscillate as they line up at the metaphase plate, alternating between orienting parallel and perpendicular to the spindle and division axis (Figure 3B, 3C). These results suggest that the parallel and perpendicular orientations of the acentric at the metaphase plate are due to the fact that they oscillate while aligning on the plate prior to anaphase onset. During anaphase, acentric sisters that are oriented parallel separate by sliding, while those oriented perpendicularly separate via unzipping [Vicars et al., 2021].

186 **Anti-parallel alignment of sister acentrics**

187 To more precisely determine acentric orientation during metaphase alignment, neuroblasts
188 expressing inducible I-CreI, the histone marker H2Av-RFP, and the telomere marker HOAP-
189 GFP [Cenci et al., 2003] were imaged live. Marked telomeres enabled us to determine the
190 orientation of paired sister acentrics with respect to one another as they aligned on the
191 metaphase plate. A surprising outcome of this analysis is that a low but notable frequency of
192 sister acentrics exhibited anti-parallel alignment. As expected, 100% (25/25) of intact
193 chromosomes have telomeres paired and aligned (Figure 4). However, in 12% (4/34) of paired
194 sister acentrics, the telomeres are oriented in opposing directions, with the remaining 88%
195 (30/34) exhibiting normal telomere-to-telomere alignment. This implies that stable pairing of
196 sister chromatids is possible despite the absence of a gene-by-gene alignment. These findings
197 indicate the kinetochore plays a key role in ensuring the fidelity of sister chromosome alignment
198 in *Drosophila*. Additionally, we find acentrics are oriented with their telomeres facing the
199 periphery of the mass of congressed chromosomes (N=10, Figure 4C & 4D).

200

201 **Acentric alignment requires microtubule plus-ends**

202 Previous studies in *Drosophila* reported the microtubule-stabilizing protein Map205 and
203 the microtubule plus-end associated protein EB1 are required for acentric sister separation
204 during anaphase initiation [Vicars et al., 2021]. To determine if acentric alignment on the
205 metaphase plate relies on microtubule plus-ends, we re-analyze published data of cells
206 expressing RNAi against the microtubule plus-end tracking protein EB1 [Vicars et al., 2021]. Our
207 analysis reveals 27% (8/30) of acentric sisters unable to align with kinetochore-bearing
208 chromosomes (Figure 5). In control wild-type cells expressing only I-CreI, only 5% of acentric
209 sisters fail to congress to the metaphase plate (Figure 5).

210

211

212 A separate study demonstrated that peripheral interpolar microtubules play a critical role
213 in the poleward segregation of acentric chromosome fragments [Karg et al., 2017]. Disruption of
214 interpolar microtubule organization via knockdown of Klp3a (kinesin-4), disrupts the poleward
215 segregation of the acentric, but not intact chromosomes. Additional laser-ablation experiments
216 demonstrated that segregating acentrics are physically connected to the interpolar microtubules
217 [Karg et al., 2017]. To determine if interpolar microtubules are involved in acentric movement to
218 and alignment on the metaphase plate, we re-analyzed previously published acentric movies in
219 a *klp3a* knockdown. *Drosophila* neuroblasts homozygous for hypomorphic alleles of *klp3a*,
220 exhibited defects in congression of the acentrics, but not the intact chromosomes (Figure 6B &
221 6C). In I-CreI expressing wild-type and *klp3a* mutant neuroblasts, 5% (1/18) and 30% (6/20) of
222 acentrics fail to align with kinetochore-bearing chromosomes at the metaphase plate
223 respectively (Figure 6C).
224 Examination of chromosome dynamics on monopolar spindles provides a means to
225 readily determine the extent to which microtubule plus-end forces act on chromosomes [Muscat
226 et al., 2015]. Unfortunately, we discovered the small molecule inhibitors commonly used to
227 induce monopolar spindles do not work in *Drosophila*. However, we find that RNAi knockdown
228 of the chromokinesin Klp31E (kinesin 4) in *Drosophila* neuroblasts resulted in monopolar spindle
229 formation. In these *Drosophila* neuroblasts with monopolar spindles, the acentric chromosomes,
230 as well as the intact chromosomes, are pushed to the cell periphery (Figure 7). This finding
231 indicates acentric chromosomes can be driven to microtubule plus ends prior to the metaphase-
232 to-anaphase transition without requiring kinetochores. It remains to be determined if the
233 acentrics are directly interacting with microtubule plus ends or utilizing motor proteins to travel to
234 the microtubule plus ends.
235 Surprisingly, despite the presence of monopolar spindles when Klp31E is partially
236 knocked down, neuroblasts form an acentrosomal bipolar spindle allowing cells to successfully
237 divide. 92% (14/15) of acentrics are able to align on the metaphase plate, with 80% (12/15) of

238 acentric sisters successfully separating and segregating from one another and moving to
239 opposite cell poles (Figure 7C & 7D).
240
241 **Discussion**
242
243 Taking advantage of our ability to fluorescently tag the *Drosophila* X-chromosome
244 acentric, we define the forces acting on the chromosome arms and the role of the kinetochore in
245 chromosome congression. These studies revealed that during the late stages of congression,
246 acentrics move faster than their neighboring kinetochore-bearing chromosomes. This indicates
247 that kinetochore microtubule interactions act as a brake during congression slowing the action
248 of plus-end directed forces acting on chromosome arms. In a similar fashion, the minus-end
249 directed kinesin, Ncd (kinesin-14), acts as a brake on the action of the plus-end directed
250 KLP61F (kinesin-5) in sliding anti-parallel microtubules during spindle pole separation [Tao et
251 al., 2006]. Thus, the kinetochore serves to modulate and reduce the motion of the
252 chromosomes during congression and alignment on the metaphase plate.
253 Our analysis also demonstrates that in contrast to intact chromosomes, the paired sister
254 acentrics oscillate during the late stages of congression and upon arrival at the metaphase
255 plate. The most likely explanation is that in the absence of a kinetochore, polar ejection forces
256 unevenly distributed along the length of the chromosome generate oscillating movements. Thus,
257 the kinetochore serves to stabilize chromosome orientation during alignment on the metaphase
258 plate. As a result of these oscillations, sister acentrics orient either parallel or perpendicular to
259 the spindle at anaphase onset. The former orientation results in acentric sister separation by
260 sliding past one another while the later results in acentrics separating via “unzipping” with
261 separation starting at one end of the chromosome [Vicars et al., 2021]
262 We also find that acentric sisters are positioned at the periphery of the metaphase plate
263 and on a plane distinct from the rest of the chromosome complement. Previous studies
264 demonstrated that the peripheral interpolar microtubules play a key role in acentric segregation

265 during anaphase [Karg et al., 2017]. The positioning of the acentrics at the edge of the
266 metaphase plate, and its association with interpolar microtubules, indicates that congression
267 and alignment of the acentric chromosomes relies on interpolar microtubules. This conclusion is
268 supported by the finding that knockdown of Klp3a, a kinesin required for establishing the
269 population of interpolar microtubules, preferentially disrupts congression of acentric
270 chromosomes [Karg et al., 2017]. *Drosophila* neuroblasts homozygous for hypomorphic alleles
271 of *klp3a*, exhibit a dramatic increase in acentric congression defects (Figure 6). Since Klp3a is a
272 chromokinesin, it is also possible that it interacts directly with acentrics propelling them along
273 interpolar microtubules to the metaphase plate. Our finding that acentrics oscillate argues
274 against this as direct lateral interactions between the acentric and microtubules would inhibit
275 oscillation. In addition, the fact that the acentrics move faster than intact chromosomes suggests
276 that they are not restricted by direct interactions with motor proteins. Acentrics may
277 preferentially rely on interpolar microtubules due to the fact that kinetochore microtubules
278 maintain intact chromosomes in a limited central region of the spindle. Lacking a kinetochore,
279 acentrics are shunted to the interpolar microtubules.
280 Our studies also demonstrate that polar ejection forces play significant roles in acentric
281 congression. This is most dramatically illustrated by the fact that reduction of EB1 activity
282 preferentially disrupts alignment of the acentric on the metaphase plate but not the intact
283 chromosomes. EB1 has been found to be essential for generating anti-polar forces on
284 chromosomes and stabilizing microtubules [Tirnauer & Bierer, 2000; Vitre et al., 2008]. This
285 finding is also supported by the finding that in monopolar spindles acentrics are rapidly pushed
286 away from the poles. As described above, the oscillation of acentrics as they align at metaphase
287 is readily explained by distributed plus-end directed forces acting along the chromosome arms.
288 One of the most surprising findings of this study emerges from live imaging paired sister
289 acentrics with GFP-labeled telomeres. The labeled telomeres enable us to determine the
290 relative orientation of each sister chromatid in the acentric pair as they align to the metaphase

plate. As expected, intact sister chromatids exhibit parallel alignment across the entire length of the chromosome. This gene-for-gene alignment of paired sisters likely facilities their stable cohesion. In addition, it is essential for successful mitotic recombination [Lisby & Rothstein, 2015; Cohen-Fix, 2001]. Surprisingly, we find that a small but significant fraction of sister acentrics align in an anti-parallel orientation, indicating that the kinetochore is required to prevent antiparallel alignment of sister chromatids. The mechanism by which the kinetochore facilitates parallel alignment remains unknown as it is likely established during interphase immediately following completion of S-phase [Skibbens, 2008].

Another unexpected finding from this analysis is that the presence of the acentric chromosome fragment induces a global reorganization of congressed chromosomes. In wild-type *Drosophila* neuroblasts, fully congressed chromosomes are roughly organized as a column at metaphase. However, in the presence of the acentric chromosome fragment, the chromosomes arrange themselves in a ring-like configuration. With a lack of chromatin in the center of the ring the congressed chromosomes form a torus. Whether it is the presence of the acentric or damaged DNA that causes the global reorganization of the congressed chromosome remains unclear. Interestingly, this torus configuration of chromosomes at metaphase is well-documented in human cells [Paulson et al., 2021]. 3D-reconstructions of human metaphase chromosomes reveal their arrangement in a circular shape with kinetochores organized around the center and chromosome arms pushed towards the cell periphery [Paulson et al., 2021]. It should be noted, that human cancer cell lines often contain damaged DNA [Lewis & Golsteyn, 2016; Valencia-González et al., 2019]. As with acentric induction in *Drosophila*, the presence of DNA damage may induce the toroidal shape of the chromosome mass at metaphase.

Studies in other species reveal distinct mechanisms can result in congressed chromosomes forming a torus. For example, a similar torus configuration of congressed chromosomes has been observed in diatoms. In these species, interpolar microtubules gather in the center of the cell at metaphase, connecting spindle poles, and push chromosomes to either

317 side of the interpolar microtubule bundle [Pickett-Heaps et al., 1975]. Additionally, in
318 prometaphase newt pneumocytes, bundles of keratin filaments push chromosomes to the cell
319 periphery [Hayden et al., 1990]. However, in *Drosophila* neuroblasts expressing I-CreI, the
320 mitotic spindle is arranged with microtubules connecting to congressed chromosomes in the
321 torus formation and an absence of microtubules in the center of the torus (Supplemental Figure
322 3). Whether the torus configuration has functional consequences or is simply an outcome of the
323 mechanisms by which the spindle is formed is unknown. Taken together, these data support a
324 model in which acentrics congress to and align on the metaphase plate via plus-end microtubule
325 interactions stabilized by outer pole-to-pole microtubules and microtubule-associated proteins.
326
327 **Materials and methods**

328 **Fly stocks**

329 All stocks were raised on standard *Drosophila* media at room temperature (20–22˚C) as
330 previously described [Royou et al., 2008]. For generating acentrics, a transgenic fly line bearing
331 the I-CreI endonuclease under heat-shock 70 promoter were kindly provided by Kent Golic at
332 The University of Utah.
333

334 **Live analysis of acentric behavior in *Drosophila* third instar neuroblasts**

335 As previously described, acentric chromosome fragments were induced by I-CreI expression
336 (under heat shock 70 promoter) in 3rd instar larvae by a 1-hour 37˚C heat shock followed by a
337 1-hour recovery period at room temperature [Royou et al., 2010]. The larval brains from third
338 instar larvae were then dissected in PBS and placed on a slide with 20 µl of PBS. A coverslip
339 was placed on the brain in PBS and the excess PBS was wicked out from the edges of the
340 coverslip to induce squashing of brain between the slide and coverslip. Then, the edge of
341 coverslip was sealed with halocarbon and was imaged for live analysis as described below.
342 Neuroblast divisions in images for Figures 1-4, 6 and 7, Table 1, and Supplemental Figure 1

343 were from male 3rd instar larvae. Neuroblast divisions in images for Figure 5 and Supplemental
344 Figure 2 were from female 3rd instar larvae.
345
346 **Microscopy and image acquisition**
347 **Wide-field microscopy.** Time-lapse imaging for Figures 5B and 5C was performed using a
348 Leica DM16000B wide-field inverted microscope equipped with a Hamamatsu electron-
349 multiplying charge coupled device camera (ORCA 9100–02) with a binning of 1 and a
350 100x Plan-Apochromat objective with NA 1.4. Successive time points were filmed at 20 second
351 intervals. RFP (585 nm) and GFP (508 nm) fluorophores were imaged. Samples were imaged in
352 PBS and at room temperature (20–22˚C). Widefield images were acquired with Leica
353 Application Suite Advanced Fluorescence Software and 3D deconvolved using AutoQuant
354 X2.2.0 software.
355 **Spinning-disk microscopy.** Images in Figures 1-4, 5A, 6, and 7, and Supplemental Figures 1
356 and 2 were acquired with an inverted Nikon Eclipse TE2000-E spinning disk (CSLI-X1) confocal
357 microscope equipped with a Hamamatsu electron-multiplying charge coupled device camera
358 (ImageEM X2) with a 100X 1.4 NA oil-immersion objective. Samples were imaged in PBS and
359 at room temperature (20–22˚C). Images were acquired with MicroManager 1.4 software. Time-
360 lapse fluorescent images of neuroblasts divisions were done with 120 and 100 ms exposures for
361 GFP and RFP respectively with 0.5 μm Z-steps. Time-lapse videos with both GFP and RFP
362 were done every 5 seconds and time-lapse movies with RFP alone were done every 5 seconds.
363 Figures were assembled in Adobe Illustrator. Selected stills (both experimental and control)
364 were processed with ImageJ (http://rsb.info.nih.gov/ij/)).
365
366 **Measurements**
367 In Figure 2, circularity measurements of chromosomes (H2Av-RFP) were done using the
368 circularity function in ImageJ of the region outlined around acentrics and the main mass of

369 chromosomes. For statistical analyses, two-sided Mann-Whitney U tests were used. Two-sided
370 Mann-Whitney U tests were performed in R (R Core Team) and Prism Version 8 (GraphPad
371 Software). 3D renderings in Figures 2 and 4 and Supplemental Figure 2 were created using
372 Imaris software.
373

374 **References**
375

376 1. Bajer A. Cine-micrographic studies on chromosome movements in β-irradiated cell.
377 Chromosoma.1958; 9:319–331. PMID: 13608834.
378
379 2. Barisic, M, Aguiar, P, Geley, S, Maiato, H. Kinetochore motors drive congression of
380 peripheral polar chromosomes by overcoming random arm-ejection forces. Nat Cell Biol.
381 2014; 16:1249–1256. https://doi.org/10.1038/ncb3060
382
383 3. Bretscher HS, Fox DT. Proliferation of Double Strand Break Resistant Polyploid Cells
384 Requires Drosophila FANCD2. Dev Cell. 2016; 37(5):444–57.
385 https://doi.org/10.1016/j.devcel.2016.05.004 PMID: 27270041; PubMed Central PMCID:
386 PMC4901310.
387
388 4. Carlson JG Mitotic behavior of induced chromosomal fragments lacking spindle
389 attachments in the neuroblasts of the grasshopper. Proc Natl Acad Sci USA. 1938a;
390 24:500–507. https://doi.org/10.1073/pnas.24.11.500
391
392 5. Cenci G, Siriaco G, Raffa GD, Kellum R, Gatti M. The Drosophila HOAP protein is
393 required for telomere capping. Nat Cell Biol. 2003; 5(1):82–4.
394 https://doi.org/10.1038/ncb902 PMID: 12510197.
395
396 6. Chmatal L., Yang K., Schultz R.M., Lampson M.A. Spatial Regulation of Kinetochore
397 Microtubule Attachments by Destabilization at Spindle Poles in Meiosis I. Curr.
398 Biol. 2015; 25:1835–1841. doi: 10.1016/j.cub.2015.05.013.
399
400 7. Cohen-Fix O. The making and breaking of sister chromatid cohesion. Cell. 2001 Jul
401 27;106(2):137-40. doi: 10.1016/s0092-8674(01)00439-1. PMID: 11511341.
402
403 8. Fenech M, Kirsch-Volders M, Natarajan AT, Surralles J, Crott JW, Parry J, et al.
404 Molecular mechanisms of micronucleus, nucleoplasmic bridge and nuclear bud
405 formation in mammalian and human cells. Mutagenesis. 2011; 26(1):125–32.
406 https://doi.org/10.1093/mutage/geq052 PMID: 21164193
407
408 9. Golic MM, Golic KG. A simple and rapid method for constructing ring-X chromosomes in
409 Drosophila melanogaster. Chromosoma. 2011; 120(2):159–64.
410 https://doi.org/10.1007/s00412-010-0297-2 PMID:21085980; PubMed Central PMCID:
411 PMC4454366.
412
413 10. Guacci V, Koshland D, Strunnikov A. A Direct Link between Sister Chromatid Cohesion
414 and Chromosome Condensation Revealed through the Analysis of MCD1 in S.

cerevisiae. Cell. 1997; 91(1):47–57. https://doi.org/10.1016/s0092-8674(01)80008-8 PMID: 9335334; PubMed Central PMCID: PMC2670185.

11. Hayden JH, Bowser SS, Rieder CL. Kinetochores capture astral microtubules during chromosome attachment to the mitotic spindle: direct visualization in live newt lung cells. J Cell Biol. 1990 Sep;111(3):1039-45. doi: 10.1083/jcb.111.3.1039. PMID: 2391359; PMCID: PMC2116290.

12. Ishii K, Ogiyama Y, Chikashige Y, Soejima S, Masuda F, Kakuma T, et al. Heterochromatin Integrity Affects Chromosome Reorganization After Centromere Dysfunction. Science. 2008; 321(5892):1088–91. https://doi.org/10.1126/science.1158699 PMID: 18719285.

13. Kanda T, Otter M, Wahl GM. Mitotic segregation of viral and cellular acentric extrachromosomal molecules by chromosome tethering. J Cell Sci. 2001; 114:49–58. PMID: 11112689.

14. Kanda T, Sullivan KF, Wahl GM Histone-GFP fusion protein enables sensitive analysis of chromosome dynamics in living mammalian cells. Curr Biol. 1998; 8:377–385. https://doi.org/10.1016/s0960-9882(98)70156-3

15. Kanda T, Wahl GM. The dynamics of acentric chromosomes in cancer cells revealed by GFP- based chromosome labeling strategies. J Cell Biochem Suppl. 2000; Suppl 35:107–14. https://doi.org/10.1002/1097-4644(2000)79:35+<107::aid-jcb1133>3.0.co;2-y PMID: 11389539.

16. Kapoor T.M., Lampson M.A., Hergert P., Cameron L., Cimini D., Salmon E.D., McEwen B.F., Khodjakov A. Chromosomes can congress to the metaphase plate before biorientation. Science. 2006;311:388–391. doi: 10.1126/science.1122142.

17. Karg T, Elting MW, Vicars H, Dumont S, Sullivan W. The chromokinesin Klp3a and microtubules facilitate acentric chromosome segregation. J Cell Biol. 2017; 216(6):1597–608. https://doi.org/10.1083/jcb.201604079 PMID: 28500183; PubMed Central PMCID: PMC5461011.

18. Karg T, Warecki B, Sullivan W. Aurora B–mediated localized delays in nuclear envelope formation facilitate inclusion of late-segregating chromosome fragments. Mol Biol Cell. 2015; 26(12):2227–41. https://doi.org/10.1091/mbc.E15-01-0026 PMID: 25877868; PubMed Central PMCID: PMC4462941.

19. Kaye JA, Melo JA, Cheung SK, Vaze MB, Haber JE, Toczyski DP. DNA breaks promote genomic instability by impeding proper chromosome segregation. Curr Biol. 2004; 14:2096–2106. https://doi.org/10.1016/j.cub.2004.10.051

20. Khodjakov A, Rieder CL. Kinetochores moving away from their associated pole do not exert a significant pushing force on the chromosome. J Cell Biol. 1996; 135:315–327. https://doi.org/10.1083/jcb.135.2.315

21. Krenn V, Musacchio A. The Aurora B Kinase in Chromosome Bi-Orientation and Spindle Checkpoint Signaling. Front Oncol. 2015 Oct 16;5:225. doi: 10.3389/fonc.2015.00225. PMID: 26528436; PMCID: PMC4607871.

22. LaFountain JR, Oldenbourg R, Cole RW, Rieder CL. Microtubule Flux Mediates Poleward Motion of Acentric Chromosome Fragments during Meiosis in Insect Spermatocytes. Mol Biol Cell. 2001; 12 (12):4054–65. https://doi.org/10.1091/mbc.12.12.4054 PMID: 11739800; PubMed Central PMCID: PMC60775.

23. Lewis CW, Golsteyn RM. Cancer cells that survive checkpoint adaptation contain micronuclei that harbor damaged DNA. Cell Cycle. 2016 Nov 16;15(22):3131-3145. doi: 10.1080/15384101.2016.1231287. Epub 2016 Sep 16. PMID: 27636097; PMCID: PMC5134707.

24. Liang H, Wright WH, Cheng S, He W, Berns MW. Micromanipulation of chromosomes in PTK2 cells using laser microsurgery (optical scalpel) in combination with laser-induced optical force (optical tweezers). Experimental cell research. 1993; 204(1):110–20. https://doi.org/10.1006/excr.1993.1015 PMID: 8416789.

25. Lisby M, Rothstein R. Cell biology of mitotic recombination. Cold Spring Harb Perspect Biol. 2015 Mar 2;7(3):a016535. doi: 10.1101/cshperspect.a016535. PMID: 25731763; PMCID: PMC4355273.

26. Maggert KA, Golic KG. Highly Efficient Sex Chromosome Interchanges Produced By I-CreI Expression in Drosophila. Genetics. 2005; 171(3):1103–14. https://doi.org/10.1534/genetics.104.040071 PMID:16020774; PubMed Central PMCID: PMC1456814.

27. Maiato H, Gomes AM, Sousa F, Barisic M. Mechanisms of Chromosome Congression during Mitosis. Biology (Basel). 2017 Feb 17;6(1):13. doi: 10.3390/biology6010013. PMID: 28218637; PMCID: PMC5372006.

28. McEwen B.F., Chan G.K., Zubrowski B., Savoian M.S., Sauer M.T., Yen T.J. CENP-E is essential for reliable bioriented spindle attachment, but chromosome alignment can be achieved via redundant mechanisms in mammalian cells. Mol. Biol. Cell. 2001; 12:2776–2789. doi: 10.1091/mbc.12.9.2776.

29. Michaelis C, Ciosk R, Nasmyth K. Cohesins: Chromosomal Proteins that Prevent Premature Separation of Sister Chromatids. Cell. 1997; 91(1):35–45. https://doi.org/10.1016/s0092-8674(01)80007-6 PMID: 9335333.

30. Muscat CC, Torre-Santiago KM, Tran MV, Powers JA, Wignall SM. Kinetochore-independent chromosome segregation driven by lateral microtubule bundles. Elife. 2015 May 30;4:e06462. doi: 10.7554/eLife.06462. PMID: 26026148; PMCID: PMC4481507.

31. Navarro AP, Cheeseman IM. Kinetochore assembly throughout the cell cycle. Semin Cell Dev Biol. 2021 Sep; 117:62-74. doi: 10.1016/j.semcdb.2021.03.008. Epub 2021 Mar 19. PMID: 33753005; PMCID: PMC8384650.

32. Ohno Y, Ogiyama Y, Kubota Y, Kubo T, Ishii K. Acentric chromosome ends are prone to fusion with functional chromosome ends through a homology-directed rearrangement. Nucleic Acids Res. 2016; 44(1):232–44. https://doi.org/10.1093/nar/gkv997 PMID: 26433224; PubMed Central PMCID: PMC4705696.

33. Paredes S, Maggert KA. Ribosomal DNA contributes to global chromatin regulation. Proc Natl Acad Sci USA. 2009; 106(42):17829–34. https://doi.org/10.1073/pnas.0906811106 PMID: 19822756; PubMed Central PMCID: PMC2764911.

34. Paulson JR, Hudson DF, Cisneros-Soberanis F, Earnshaw WC. Mitotic chromosomes. Semin Cell Dev Biol. 2021 Sep;117:7-29. doi: 10.1016/j.semcdb.2021.03.014. Epub 2021 Apr 6. PMID: 33836947; PMCID: PMC8406421.

35. Pickett-Heaps JD, McDonald KL, Tippit DH. Cell division in the pennate diatom Diatom vulgare. Protoplasma. 1975; 86, 205-242.

36. Platero JS, Ahmad K, Henikoff S. A Distal Heterochromatic Block Displays Centromeric Activity When Detached from a Natural Centromere. Molecular Cell. 1999; 4(6):995–1004. https://doi.org/10.1016/s1097-2765(00)80228-2 PMID: 10635324.

37. Porter ACG, Farr CJ. Topoisomerase II: untangling its contribution at the centromere. Chromosome Res. 2004; 12(6):569–83. https://doi.org/10.1023/B:CHRO.0000036608.91085.d1 PMID: 15289664.

38. Rieder CL, Davison EA, Jensen LC, Cassimeris L, Salmon ED. Oscillatory movements of monooriented chromosomes and their position relative to the spindle pole result from the ejection properties of the aster and half-spindle. J Cell Biol. 1986 Aug;103(2):581-91. doi: 10.1083/jcb.103.2.581. PMID: 3733881; PMCID: PMC2113830.

39. Rong YS, Titen SW, Xie HB, Golic MM, Bastiani M, Bandyopadhyay P, et al. Targeted mutagenesis by homologous recombination in D. melanogaster. Genes Dev. 2002; 16(12):1568–81. https://doi.org/10.1101/gad.986602 PMID: 12080094; PubMed Central PMCID: PMC186348.

40. Royou A, Gagou ME, Karess R, Sullivan W. BubR1- and Polo-Coated DNA Tethers Facilitate Poleward Segregation of Acentric Chromatids. Cell. 2010; 140(2):235–45. https://doi.org/10.1016/j.cell.2009.12.043 PMID: 20141837; PubMed Central PMCID: PMC2969851.

41. Royou A, McCusker D, Kellogg DR, Sullivan W. Grapes (Chk1) prevents nuclear CDK1 activation by delaying cyclin B nuclear accumulation. J Cell Biol. 2008; 183(1):63–75. https://doi.org/10.1083/jcb.200801153 PMID: 18824564; PubMed Central PMCID: PMC2557043.

42. Skibbens RV. Mechanisms of sister chromatid pairing. Int Rev Cell Mol Biol. 2008;269:283-339. doi: 10.1016/S1937-6448(08)01005-8. PMID: 18779060.

43. Sural TH, Peng S, Li B, Workman JL, Park PJ, Kuroda MI. The MSL3 chromodomain directs a key targeting step for dosage compensation of the Drosophila melanogaster X chromosome. Nat Struct Mol Biol. 2008 Dec;15(12):1318-25. doi: 10.1038/nsmb.1520. Epub 2008 Nov 23. PMID: 19029895; PMCID: PMC2636508.

44. Tanaka TU. Bi-orienting chromosomes: acrobatics on the mitotic spindle. Chromosoma. 2008 Dec;117(6):521-33. doi: 10.1007/s00412-008-0173-5. Epub 2008 Aug 2. PMID:

18677502.

45. Tao L, Mogilner A, Civelekoglu-Scholey G, Wollman R, Evans J, Stahlberg H, Scholey JM. A homotetrameric kinesin-5, KLP61F, bundles microtubules and antagonizes Ncd in motility assays. Curr Biol. 2006 Dec 5;16(23):2293-302. doi: 10.1016/j.cub.2006.09.064. PMID: 17141610.

46. Tirnauer JS, Bierer BE. EB1 proteins regulate microtubule dynamics, cell polarity, and chromosome stability. J Cell Biol. 2000; 149(4):761–6. https://doi.org/10.1083/jcb.149.4.761 PMID: 10811817; PubMed Central PMCID: PMC2174556.

47. Valencia-González HA, Ruíz G, Ortiz-Sánchez E, García-Carrancá A. Cancer Stem Cells from Tumor Cell Lines Activate the DNA Damage Response Pathway after Ionizing Radiation More Efficiently Than Noncancer Stem Cells. Stem Cells Int. 2019 Apr 3;2019:7038953. doi: 10.1155/2019/7038953. PMID: 31073313; PMCID: PMC6470433.

48. Vicars H, Karg T, Warecki B, Bast I, Sullivan W. Kinetochore-independent mechanisms of sister chromosome separation. PLOS Genetics. 2021; 17(1): e1009304. doi:10.1371/journal.pgen.1009304 PMID: 33513180

49. Vitre B, Coquelle FM, Heichette C, Garnier C, Chre´ tien D, Arnal I. EB1 regulates microtubule dynamics and tubulin sheet closure in vitro. Nat Cell Biol. 2008; 10(4):415–21. https://doi.org/10.1038/ncb1703 PMID: 18364701.

50. Warecki B, Sullivan W. Micronuclei formation is prevented by Aurora B-mediated exclusion of HP1a from late-segregating chromatin in Drosophila. Genetics. 2018; 210(1):171–187. https://doi.org/10.1534/genetics.118.301031 PMID: 29986897; PubMed Central PMCID: PMC6116970.

51. Warecki B, Sullivan W. Mechanisms driving acentric chromosome transmission. Chromosome Res. 2020; 28(3-4):229-246. https://doi.org/10.1007/s10577-020-09636-z PMID: 32712740.

52. Ye A.A., Deretic J., Hoel C.M., Hinman A.W., Cimini D., Welburn J.P., Maresca T.J. Aurora A Kinase Contributes to a Pole-Based Error Correction Pathway. Curr. Biol. 2015; 25:1842–1851. doi: 10.1016/j.cub.2015.06.021.

53. Yen T.J., Li G., Schaar B.T., Szilak I., Cleveland D.W. CENP-E is a putative kinetochore motor that accumulates just before mitosis. Nature. 1992;359:536–539. doi: 10.1038/359536a0.

Figure Legends

Table 1: Average velocities of chromosomes at the metaphase plate. (A) Average velocities of individual chromosomes as they align at the metaphase plate. Velocity is measured in nanometers per second. Asterisks indicate statistical significance (*P=0.005, **P=0.01) as determined by a two-sided Mann-Whitney U test. (B) Schematic showing how chromosome velocity is determined. Velocity is defined as beginning 80 seconds prior to anaphase onset and ends one frame (5 s) prior to anaphase onset.

Figure 1: Acentrics align on the metaphase plate. (A) Still frames of a time-lapse movie of a mitotic neuroblast labeled with H2Av-RFP (magenta) and MSL3-GFP (green) not expressing I-CreI. (B) Still frames of a time-lapse movie of a mitotic neuroblast with I-CreI induced acentrics. Sister acentrics (white arrowheads) undergo movement at the metaphase plate while aligning (yellow brackets), lag on the spindle equator but eventually separate, segregate, and are incorporated into daughter nuclei. Bars, 2 µm. Time in seconds.

Figure 2: Acentric induction induces a global reorganization of congressed chromosomes such that the acentric localizes to the periphery of the main chromosome mass (A) Still images of a 3D rendering of a neuroblast at metaphase labeled with H2Av-RFP (magenta) and an intact MSL3-GFP (green) tagged X chromosome (I-CreI not induced). (B) Still frames of a 3D rendering of a neuroblast at metaphase with I-CreI induced acentrics. This results in a dramatic global reorganization of the congressed chromosomes into a ring with an absence of chromatin in the center. The acentric localizes to the outer most edge of the chromosome ring. Bars, 2 µm. Images are rotated 180°. (C) Box plot showing the distances of X chromosomes from the chromosome mass center. Distances are measured in µm. Acentric X chromosomes are positioned significantly farther from the chromosome mass center when compared to the intact X chromosome (*P=0.01, Mann-Whitney Test).

Figure 3: Acentrics undergo varied orientations during metaphase (A) Still frames of a time-lapse movie of a mitotic neuroblast labeled with H2Av-RFP (magenta) and MSL3-GFP (green), not expressing I-CreI, during metaphase. Zoomed in images show only the X chromosomes marked by MSL3-GFP (gray). (B) Still frames of a time-lapse movie of a mitotic neuroblast with I-CreI induced acentrics during metaphase. Zoomed in images show only the X chromosomes marked by MSL3-GFP (gray). Bars, 2 µm. Time in seconds. (C) Line graph showing the change in orientation of acentric (green) and intact (black) X chromosomes over time, prior to anaphase onset. Data points every 5 seconds. Shaded regions represent one- and two-times the standard deviation.

Figure 4: Acentrics align at the metaphase plate with telomeres either paired or unpaired. (A) Still frames of a time-lapse movie of a mitotic neuroblast labeled with H2AvRFP (magenta) and HOAP-GFP (green) expressing I-CreI with acentric sister telomeres aligned and paired (arrowheads and yellow outline) at metaphase. (B) Still frames of a time-lapse movie of a mitotic neuroblast expressing I-CreI with acentric sister telomeres opposed (arrowheads and yellow outline) at metaphase. Most acentrics are oriented with their telomeres paired during metaphase. Bars, 2 µm. Time in seconds. (C) Still images of a 3D rendering of a mitotic neuroblast with H2Av-RFP (magenta) and HOAP-GFP (green) (N=5). (D) Still images of a 3D rendering of a mitotic neuroblast with I-CreI induced chromosome fragments. All chromosomes are arranged in a semi-circular formation with distally oriented telomeres immediately prior to anaphase onset (N=10). Bars, 2 µm. Images are rotated 180°. (E) Schematic showing frequency of sister acentrics with telomeres paired vs. telomeres opposing.

Figure 5: EB1 required for acentric metaphase plate alignment. (A) Still frames of a time-lapse movie of a mitotic neuroblast labeled with H2Av-RFP (gray) with I-CreI induced acentrics (white arrowheads). (B) Still frames of a time-lapse movie of a mitotic neuroblast expressing I-CreI and EB1 RNAi. Sister acentrics fail to align with the chromosome mass at metaphase and segregate to the same cell pole. Bars, 2 µm. Time in seconds. (C) Bar graph showing congression failure rates. Successful chromosome congression is in gray. Failure of chromosomes to congress is in magenta.

Figure 6: The chromokinesin Klp3a is required for aligning acentrics to the metaphase plate. (A) Still images from a time-lapse movie of a neuroblast expressing I-CreI alone (control). (B) Still images from a time-lapse movie of a neuroblast expressing I-CreI in *klp3a* mutant background. Acentric sisters (white arrows) are positioned near the spindle pole at metaphase. Bars, 2 μm. Time in seconds. (C) Bar graph showing the rate of chromosome alignment at the metaphase plate. Successful chromosome alignment at the metaphase plate is in gray. Failure of chromosomes to align is in magenta.

Figure 7: Acentrics are pushed by microtubule plus-ends (A) Still frames of a time-lapse movie of a mitotic neuroblast expressing H2AvRFP (magenta) and Jupiter-GFP-labeled microtubules (green) with I-CreI induced acentrics. Sister acentrics (white arrowheads) align on the metaphase plate and lag behind at the spindle equator but eventually separate, segregate, and are incorporated into daughter nuclei. (B) Still frames of a time-lapse movie of a mitotic neuroblast with I-CreI induced acentrics (white arrowheads) and expressing Klp31E RNAi. All chromosomes are pushed to the cell periphery by the mono-polar mitotic spindle. Bars, 2 μm. Time in seconds. (C) Percentages of acentric sisters that fail to congress to the metaphase plate. (D) Percentages of acentric sisters that fail to separate from one another during late anaphase.

Figure 8: Schematic showing proposed mechanism of acentric chromosome congression. Chromosomes in magenta, microtubules in green, dynein in purple, chromokinesins in orange, CENP-E in blue, and EB1 in yellow. (A) Normal chromosomes congress to the metaphase plate either through direct congression or peripheral congression. Direct congression relies on chromokinesins localized at chromosome arms and end-on kinetochore-microtubule attachments. Peripheral congression involves chromosomes initially moving to the spindle pole by the minus-end motor protein dynein. Once at the pole, the chromosomes engage chromokinesins and the kinetochore-associated kinesin CENP-E for transport to the metaphase plate. (B) Acentric chromosome fragments congress by using EB1-driven microtubule plus-end pushing forces and lateral attachments with microtubules (potentially via chromokinesins).

Table 1

A

	Avg velocity ± SD (nm/s)	N (individual chromosomes)
Intact X chromosomes	8.4 ± 3.3	12
Non-X chromosomes	8.5 ± 2.4	28
Acentric X chromosomes	11.7 ± 3.5	14

B

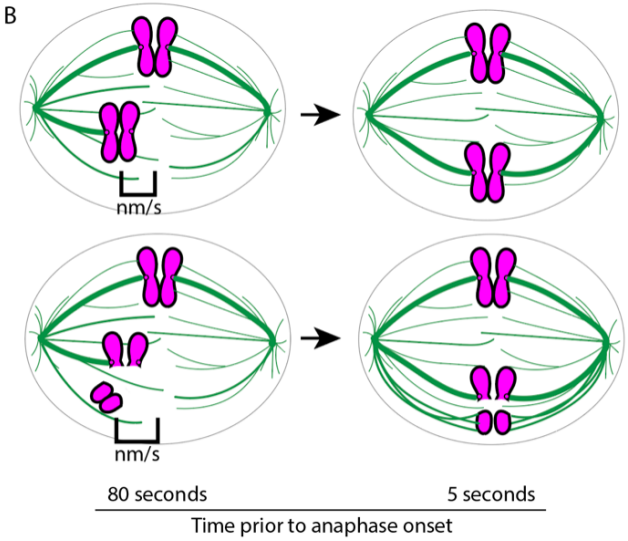

Figure 1

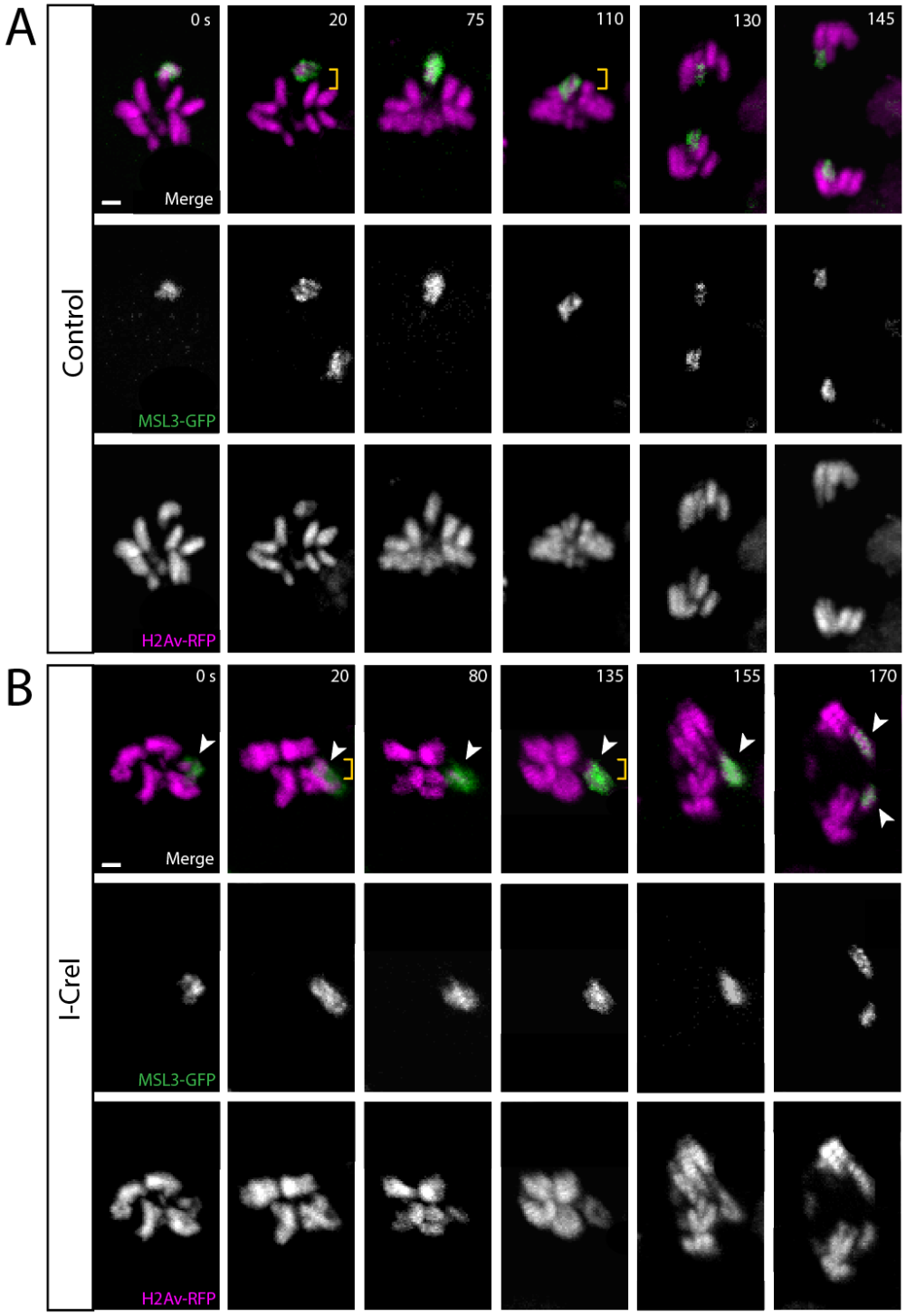
A
Control
0 s
20
75
110
130
145
Merge
MSL3-GFP
H2Av-RFP
B
I-CreI
0 s
20
80
135
155
170
Merge
MSL3-GFP
H2Av-RFP

Figure 2

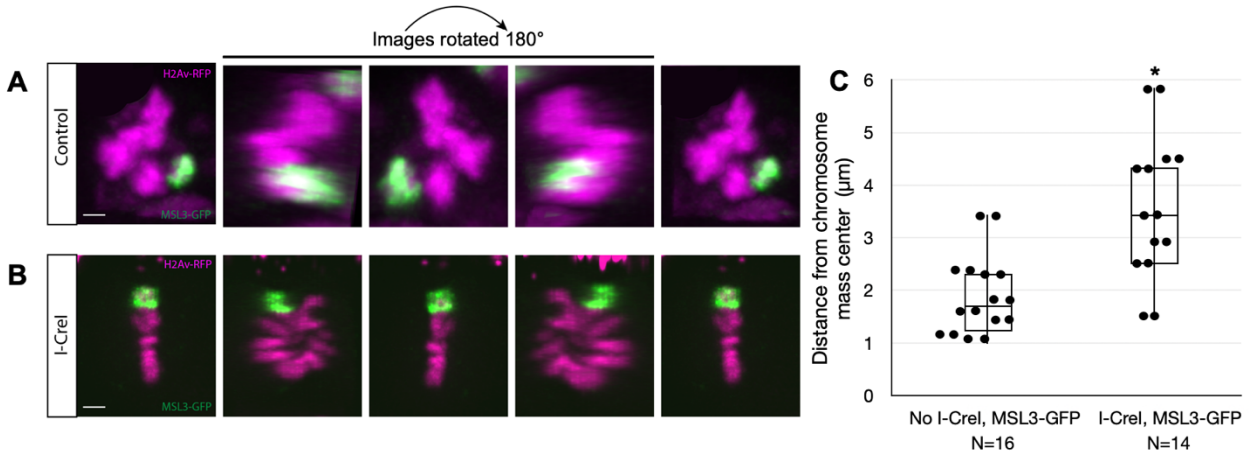

Figure 3

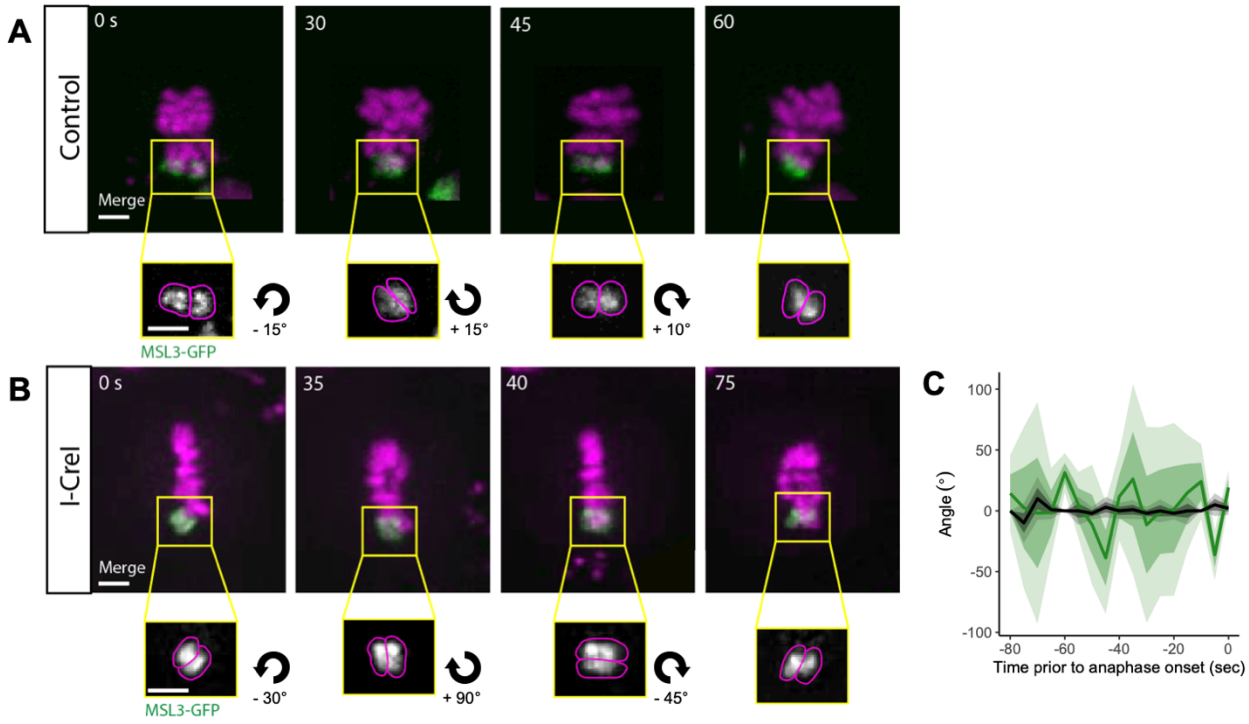

Figure 4

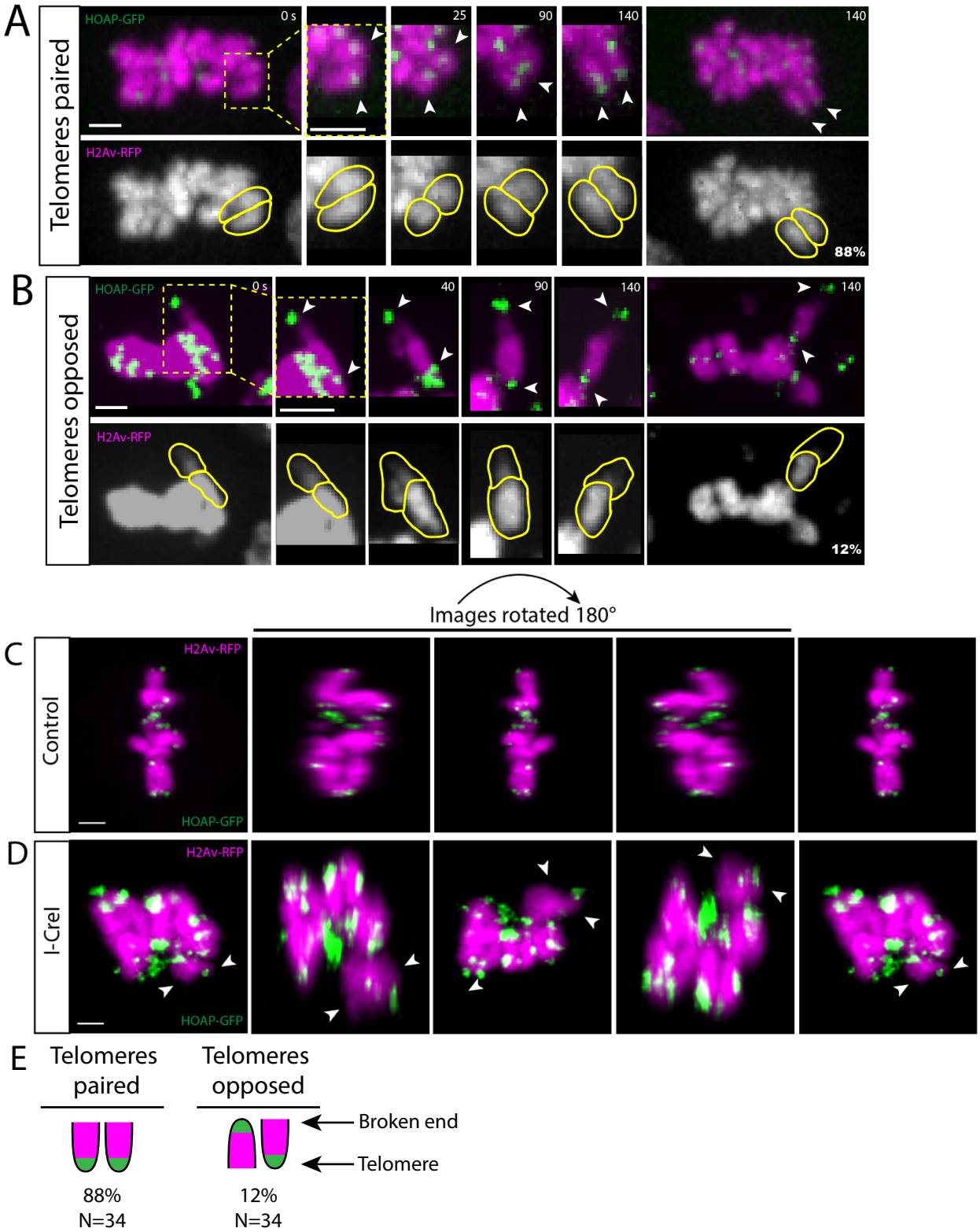
A
Telomeres paired
HOAP-GFP
H2Av-RFP
0 s
25
90
140
140
88%
B
Telomeres opposed
HOAP-GFP
H2Av-RFP
0 s
40
90
140
140
12%
Images rotated 180°
C
Control
H2Av-RFP
HOAP-GFP
D
I-CreI
H2Av-RFP
HOAP-GFP
E
Telomeres paired
Telomeres opposed
Broken end
Telomere
88%
N=34
12%
N=34

Figure 5

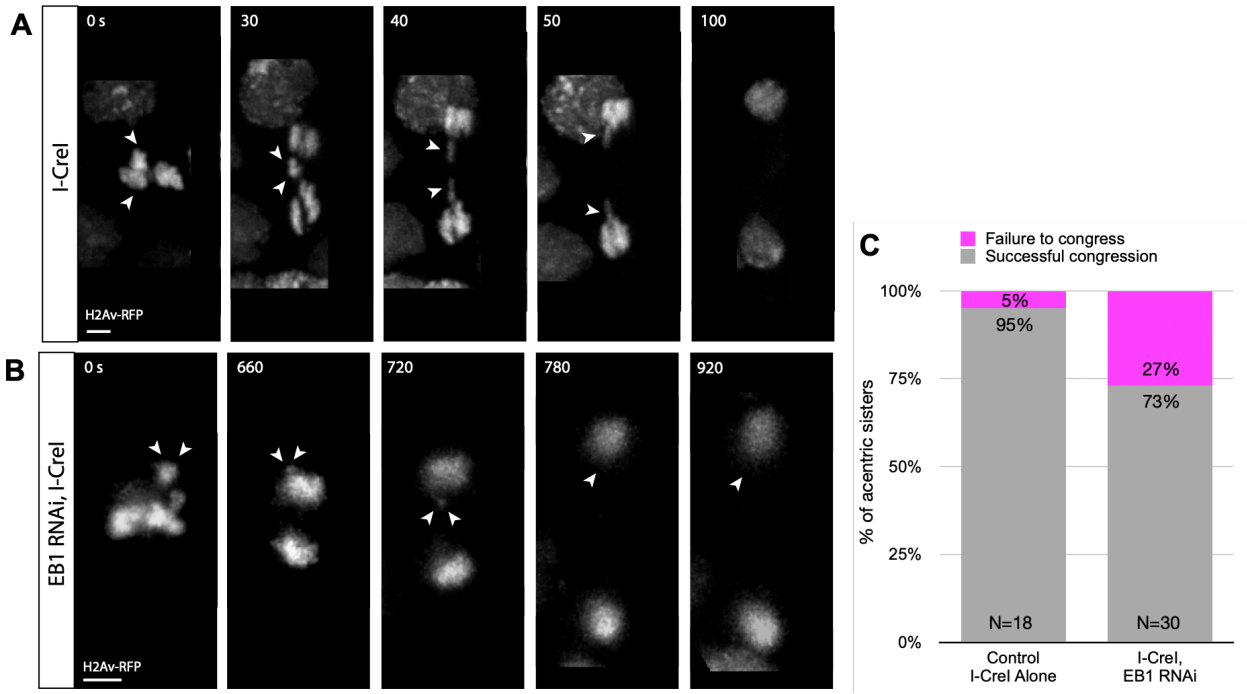

Figure 6

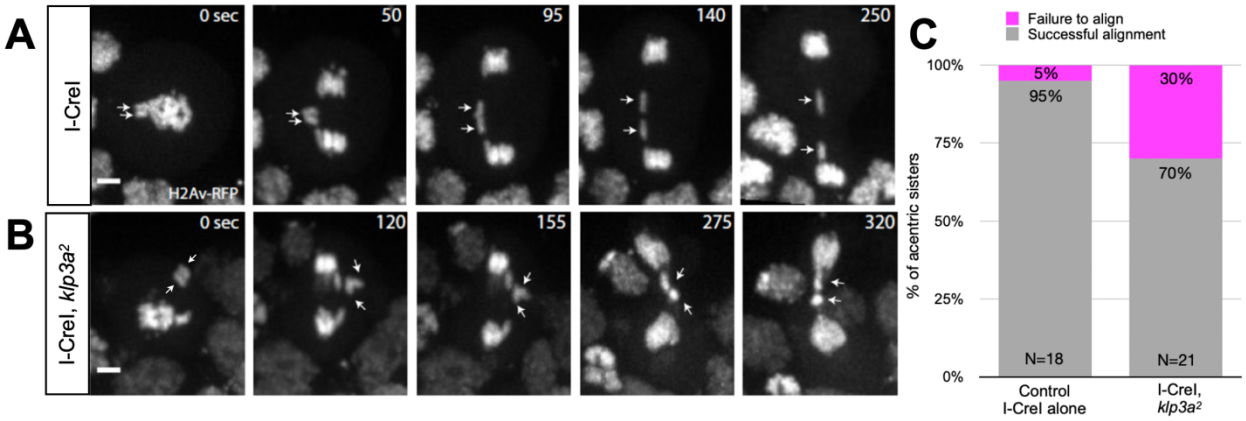

Figure 7

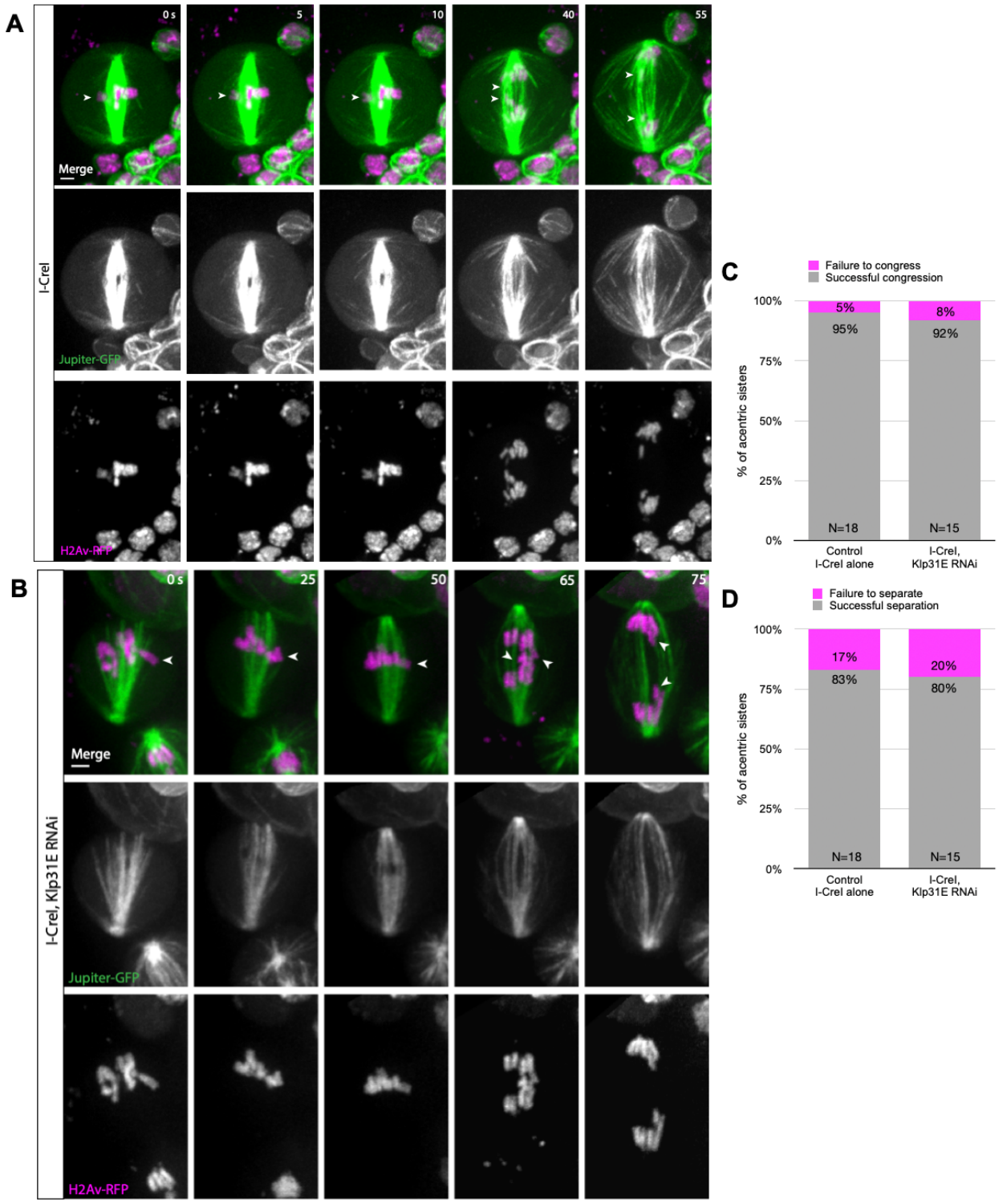
A
I-CreI
0 s
5
10
40
55
Merge
Jupiter-GFP
H2Av-RFP
B
I-CreI, Klp31E RNAi
0 s
25
50
65
75
Merge
Jupiter-GFP
H2Av-RFP
C
Failure to congress
Successful congression
% of acentric sisters
100%
75%
50%
25%
0%
5%
95%
8%
92%
N=18
N=15
Control
I-CreI alone
I-CreI,
Klp31E RNAi
D
Failure to separate
Successful separation
% of acentric sisters
100%
75%
50%
25%
0%
17%
83%
20%
80%
N=18
N=15
Control
I-CreI alone
I-CreI,
Klp31E RNAi

Figure 8

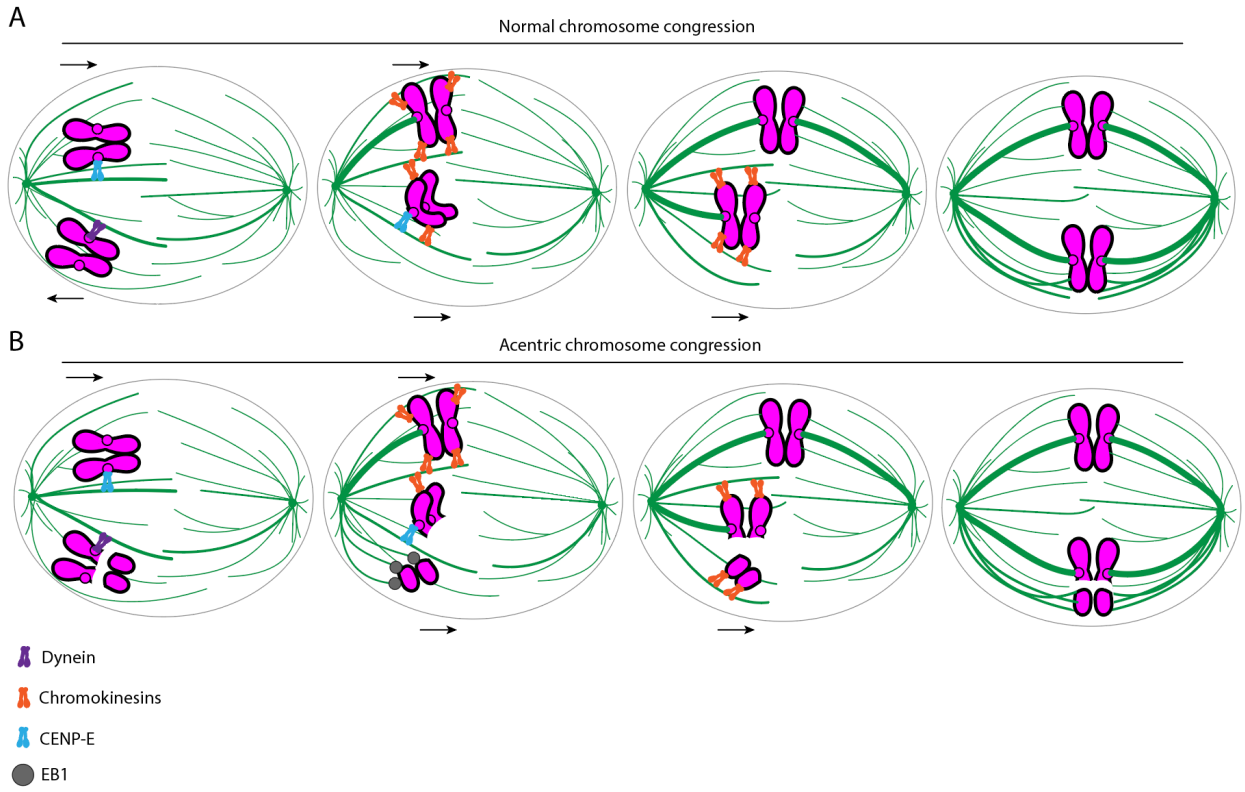
A
Normal chromosome congression
B
Acentric chromosome congression
Dynein
Chromokinesins
CENP-E
EB1